JCB Article

The raft-associated protein MAL is required for maintenance of proper axon–glia interactions in the central nervous system

Nicole Schaeren-Wiemers,[1] Annick Bonnet,[2] Michael Erb,[1] Beat Erne,[1] Udo Bartsch,[3] Frances Kern,[1] Ned Mantei,[2] Diane Sherman,[4] and Ueli Suter[2]

[1]Neurobiology, Department of Research, University Hospital Basel, 4056 Basel, Switzerland
[2]Institute of Cell Biology, Department of Biology, Swiss Federal Institute of Technology, ETH-Hönggerberg, 8093 Zürich, Switzerland
[3]Center for Molecular Neurobiology Hamburg (ZMNH) and Department of Ophthalmology, University of Hamburg, 20146 Hamburg, Germany
[4]Center for Neuroscience Research, University of Edinburgh, Edinburgh EH9 1QH, Scotland, UK

The myelin and lymphocyte protein (MAL) is a tetraspan raft-associated proteolipid predominantly expressed by oligodendrocytes and Schwann cells. We show that genetic ablation of *mal* resulted in cytoplasmic inclusions within compact myelin, paranodal loops that are everted away from the axon, and disorganized transverse bands at the paranode–axon interface in the adult central nervous system. These structural changes were accompanied by a marked reduction of contactin-associated protein/paranodin, neurofascin 155 (NF155), and the potassium channel Kv1.2, whereas nodal clusters of sodium channels were unaltered. Initial formation of paranodal regions appeared normal, but abnormalities became detectable when MAL started to be expressed. Biochemical analysis revealed reduced myelin-associated glycoprotein, myelin basic protein, and NF155 protein levels in myelin and myelin-derived rafts. Our results demonstrate a critical role for MAL in the maintenance of central nervous system paranodes, likely by controlling the trafficking and/or sorting of NF155 and other membrane components in oligodendrocytes.

Introduction

Sorting of proteins and lipids by lipid rafts has emerged as a crucial regulatory mechanism in polarized cells. Myelinating cells, oligodendrocytes in the central nervous system (CNS), and Schwann cells in the peripheral nervous system (PNS) are faced with particular challenges in this regard. Both cell types are specialized polarized cells that form the unique multilayered plasma membrane structure myelin, divided into a number of subdomains with distinct protein and lipid compositions (Arroyo and Scherer, 2000; Salzer, 2003). Extraordinary amounts of membrane proteins and lipids have to be synthesized, correctly transported, and targeted by myelinating glia during myelination in development and regeneration. Transport of proteins is directed to different myelin domains through distinct forms of detergent-insoluble glycolipid-enriched complexes (DIGs, rafts) in a highly regulated process (Kim et al., 1995; Koch et al., 1997; Kramer et al., 1997, 1999; Frank et al., 1998; Kim and Pfeiffer, 1999; Simons et al., 2000; Erne et al., 2002). This involves rafts that contain proteins guiding early development, and rafts involved in the formation of compact myelin. Fine-tuning of this elaborate system is likely achieved by reciprocal interactions between myelinating glia and axons that determine the degree of cellular polarization.

The myelin and lymphocyte protein (MAL; VIP17/MVP17) shows unique features that make it a tantalizing candidate

N. Schaeren-Wiemers and A. Bonnet contributed equally to this paper.

Address correspondence to Nicole Schaeren-Wiemers, Neurobiology, Dept. of Research, University Hospital Basel, Pharmacenter, Klingelbergstr. 50, 4056 Basel, Switzerland. Tel.: (41) 61-267-15-41. Fax: (41) 61-267-16-28. email: Nicole.Schaeren-Wiemers@unibas.ch

A. Bonnet's present address is Kanzlei DF-MP, Munich, Germany.

Key words: axon–glia interaction; myelin proteolipids; glycolipid-enriched microdomains; node of Ranvier

Abbreviations used in this paper: Caspr, contactin-associated protein/paranodin; CGT, ceramide galactosyl transferase; CNS, central nervous system; DIG, detergent-insoluble glycolipid-enriched complex; GalC, galactosylceramide; KO, knockout; L-MAG, large myelin-associated glycoprotein isoform; MAG, myelin-associated glycoprotein; MAL, myelin and lymphocyte protein; MBP, myelin basic protein; MOG, myelin oligodendrocyte glycoprotein; NaCh, sodium channel; NF, neurofascin; PLP, proteolipid protein; PNS, peripheral nervous system; WT, wild type.

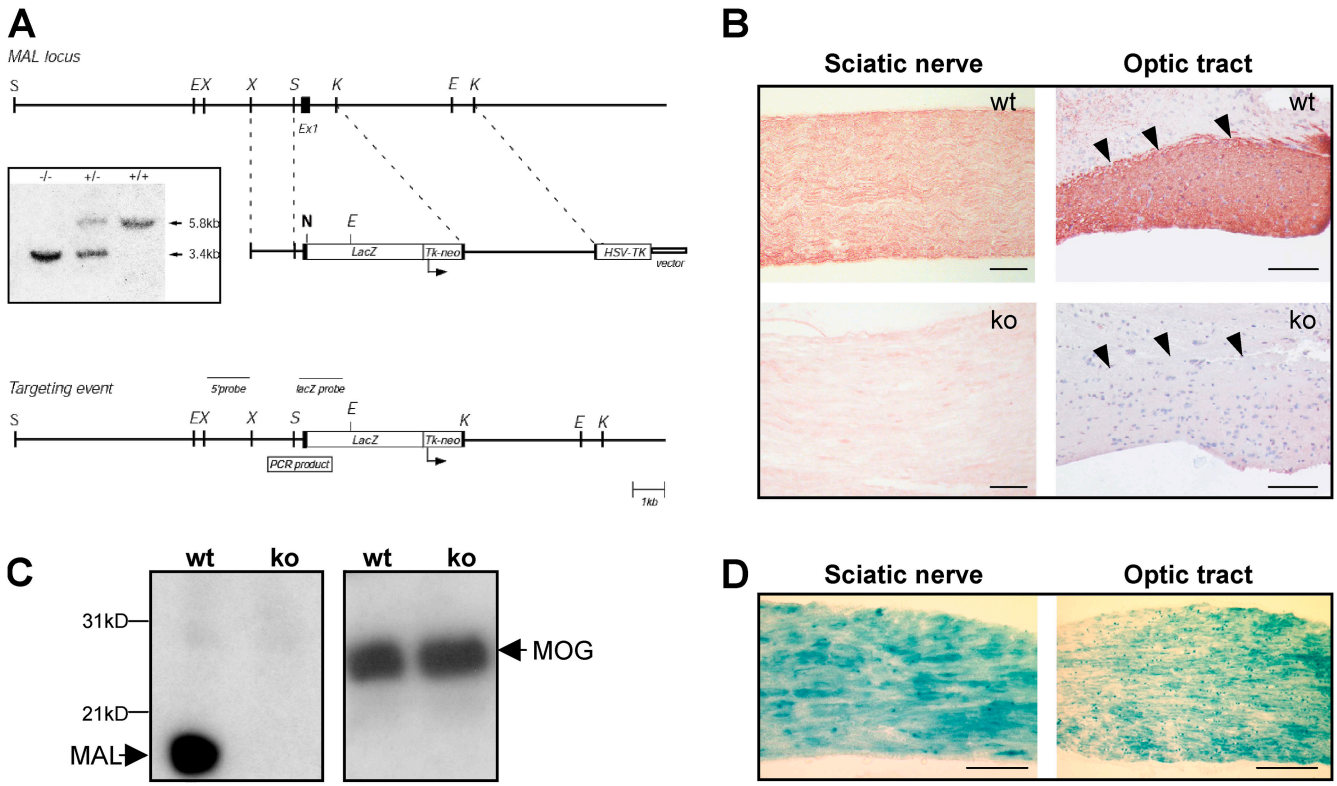

Figure 1. **Targeted disruption of the *mal* locus and generation of a *mal* KO mouse line.** (A) Partial restriction map of the *mal* locus (top), and schematic representation of the targeting construct (middle) and the targeted locus (bottom). Homologous recombination results in the concomitant deletion of exon 1 (Ex1) and insertion of a LacZ/Neo cassette that follows an artificially generated NotI site after the 3rd amino acid of the *mal* ORF in the targeting construct. HSV-Tk: herpes simplex virus thymidine kinase gene. E, X, S, and K: EcoRV, XbaI, SacII, and KpnI, respectively. Bar, 1 kb. Inset: Southern blot analysis of DNA isolated from tail biopsies, digested with EcoRV. The blot was probed with a radioactively labeled XbaI–XbaI fragment (indicated in A as 5′ probe). A 3.4-kb fragment indicates a mutant allele (−/−), whereas a 5.8-kb fragment represents a WT allele (+/+). (B) Immunohistochemistry for MAL on tissue sections from sciatic nerve and optic tract of 3-mo-old WT (top panels) and KO (bottom panels) mice. Arrowheads demarcate the border between optic tract and brain. Bars, 100 μm. (C) Western blot analysis of myelin membranes from 3-mo-old WT and KO mice using antibodies to MAL (left) and MOG (right). (D) β-Galactosidase activity, detected by X-Gal staining, in homozygous mice. Bars, 100 μm.

for regulating the sorting and/or trafficking of particular membrane components in myelinating cells (Frank, 2000). MAL is a nonglycosylated integral membrane protein highly enriched in CNS and PNS myelin (Schaeren-Wiemers et al., 1995a,b). The proteolipid MAL is also a component of lipid rafts in myelinating cells and is associated with glycosphingolipids. These MAL–glycosphingolipid interactions are believed to result in the formation of protein–lipid microdomains in myelin (Frank et al., 1998). Furthermore, MAL is enriched in rafts and apical membranes of epithelial cells (Zacchetti et al., 1995; Frank et al., 1998). Functional in vitro analyses suggest that MAL is required for apical protein sorting in epithelia (Cheong et al., 1999; Puertollano et al., 1999; Martin-Belmonte et al., 2000). Transgenic mice with increased MAL gene dosage revealed alterations of both axon–glia interaction and apical membrane formation in kidney and stomach (Frank et al., 2000). Together, the available data suggest that MAL is involved in the assembly and targeting of apical transport vesicles and in the stabilization and maintenance of glycosphingolipid-rich membrane domains.

We have tested the function of MAL in vivo by generating mice lacking this protein and found that such animals are viable and have a normal life span. The mice appeared grossly normal, but closer inspection revealed defects in the maintenance of multiple domains of myelinated CNS axons, indicating aberrant protein trafficking and/or sorting in *mal*-deficient oligodendrocytes.

Results

Generation and validation of *mal*-deficient mice

We used embryonic stem cell technology to generate *mal*-deficient mice by replacing the first exon of the *mal* gene with a *lacZ* gene (Fig. 1 A). Southern blot analysis of tail genomic DNA yielded a 5.8-kb EcoRV fragment for the wild-type (WT) allele and a diagnostic 3.4-kb EcoRV fragment for the knockout (KO) allele (Fig. 1 A, inset). Northern blot analysis of brain RNA revealed that the expression of full-length MAL mRNA was abolished in homozygous mice, whereas the LacZ-containing transcript was expressed in both heterozygous and homozygous mutant mice (unpublished data). Lack of MAL protein was shown by immunohistochemistry with an affinity-purified polyclonal anti-MAL rabbit serum on sections from sciatic nerves and brain of 3-mo-old KO animals (Fig. 1 B). We found strong MAL expression in my-

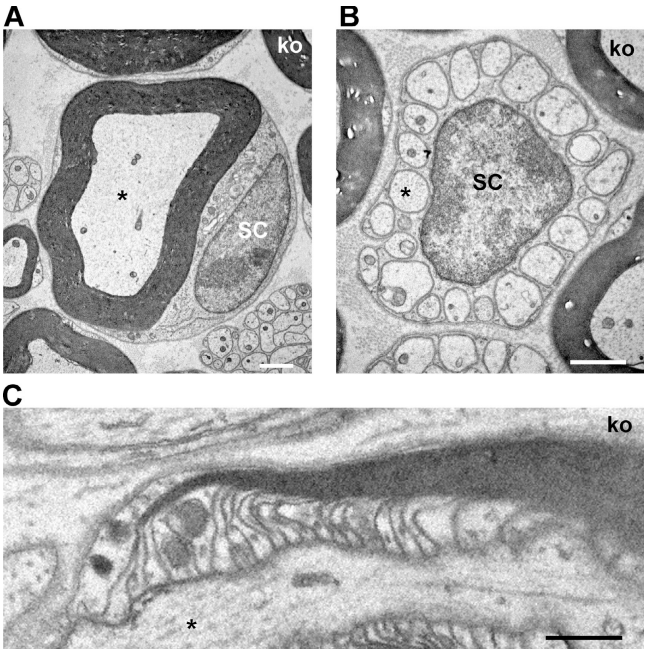

Figure 2. **Normal peripheral nerves in *mal*-deficient mice.** Morphology of sciatic nerves from 2.5-mo-old KO mice. EM analysis of cross-sectioned sciatic nerve tissues shows normal myelinated (A) and unmyelinated (B) axons of *mal* KO mice. (C) Longitudinal section of a sciatic nerve shows normal paranodal morphology in KO. Asterisk indicates an axon. SC indicates a Schwann cell body. Bars: A, 50 μm; B, 1 μm; C, 0.5 μm.

elin of sciatic nerve and optic tract from WT mice (Fig. 1 B, top). In contrast, MAL immunoreactivity was abolished in KO animals (Fig. 1 B, bottom). Absence of MAL was further confirmed by Western blot analysis of myelin preparations from WT and KO mice (Fig. 1 C). X-gal staining revealed β-galactosidase activity in sciatic and optic nerves of heterozygous and homozygous mice (Fig. 1 D).

Peripheral nerves of *mal*-deficient mice

MAL is highly expressed by Schwann cells in developing and adult peripheral nerves (Fig. 1 B). Furthermore, mice overexpressing MAL showed progressive segregation of unmyelinated PNS axons (Frank et al., 2000). Thus, we examined the sciatic nerves of 2-mo-old KO mice (Fig. 2). No significant alterations of myelinated fibers (Fig. 2 A) and nonmyelinating Schwann cells engulfing small caliber axons (Fig. 2 B, asterisk) were found. In addition, we used teased sciatic nerve fiber preparations to assess the integrity of nodes of Ranvier by immunostaining with the paranodal marker E-cadherin, contactin-associated protein/paranodin (Caspr), and the juxtaparanodal marker Kv1.1. No major changes were detected in the KO mice (unpublished data). Ultrastructural analysis of nodal and paranodal regions of PNS fibers revealed a normal morphology (Fig. 2 C). We conclude that MAL is not essential for the formation of peripheral nerves.

MAL deficiency leads to aberrantly myelinated fibers in the CNS

High levels of MAL protein were found in all myelinated fiber tracts including the optic nerve (Fig. 1 B). EM analysis

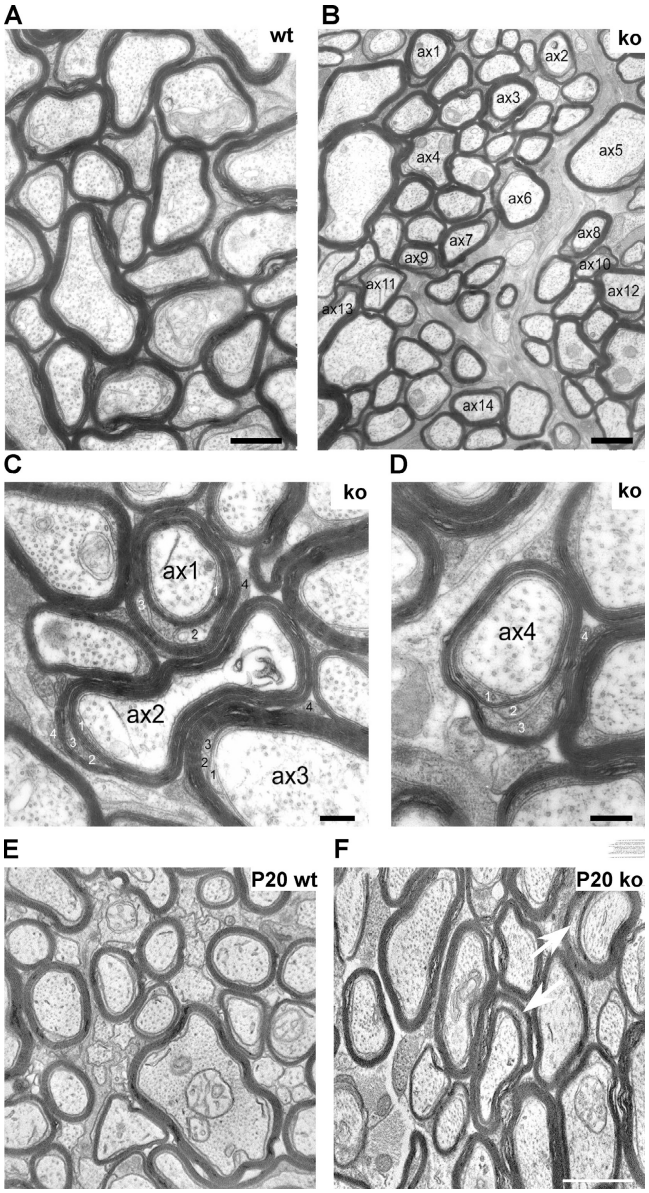

Figure 3. **Cytoplasmic inclusions in compact CNS myelin of *mal* KO mice.** EM analysis of optic nerves from WT and age-matched KO mice in adult (A–D) and during development (E and F). (A) Myelin sheaths in WT mice lack oligodendrocytic cytoplasmic inclusions in compact myelin, and the majority of sheaths display a well-developed periaxonal cytoplasmic collar that spans more than half of the axonal circumference. In *mal* KO, in contrast, many axons (ax1–ax14 in B; ax1–ax3 in C; ax4 in D) are surrounded by sheaths that contain cytoplasmic inclusions in compact myelin. Most sheaths lack a well-developed periaxonal cytoplasmic collar (B–D). Close inspection of KO sheaths at higher magnification suggests that some cytoplasmic inclusions are indicative of the presence of two myelin sheaths concentrically surrounding the same axon. Inner and outer sheaths are either spiraling in opposite directions (ax1 and ax2 in C; ax4 in D) or in the same direction (ax3 in C). (C and D) 1 and 3 indicate the inner tongue process of the inner and outer myelin sheath, respectively; 2 and 4 indicate the external tongue process of the inner and outer myelin sheath, respectively. (E and F) EM analysis of optic nerve during development at P20. Note the similar extent of myelination in WT and KO mice. Inclusions of cytoplasm within the compact myelin of KO mice were frequent at P20 (F, arrows). Although myelination in KO mice appeared less homogenous, no difference in myelin sheath thickness or in number of myelinated fibers was observed between genotypes. Bars: A, 0.5 μm; B, E, and F, 1 μm; C and D, 0.2 μm.

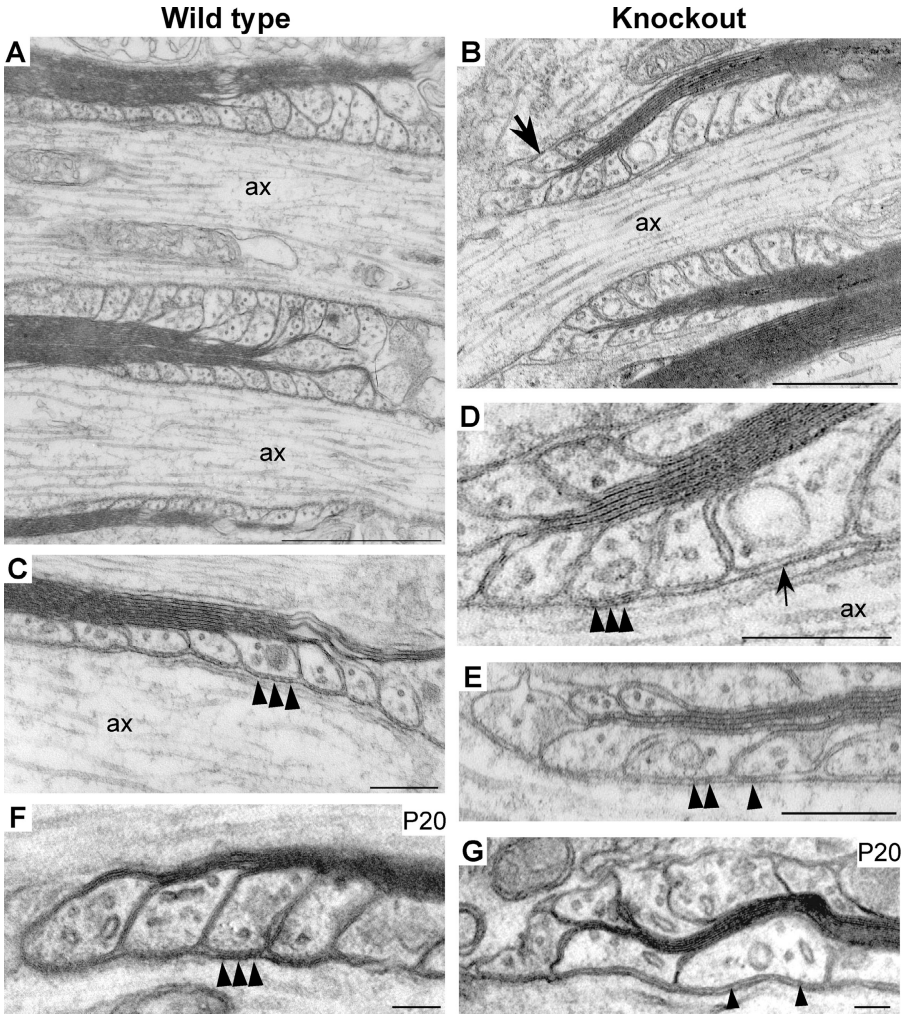

Figure 4. ***Mal*-deficient mice exhibit paranodal abnormalities.** EM analysis of longitudinally sectioned optic nerves from adult KO mice revealed numerous disorganized paranodes with everted paranodal loops not adhering to the axon (B, D, E; arrow in B). In WT animals, normal paranodal loop organization was observed (A and C). Transverse bands were regularly detected in WT mice (C, arrowheads), whereas in KO mice transverse bands were usually present but less organized (D and E, arrowheads), or absent under some of the paranodal loops (D, arrow). In the paranode in D, there is only one loop with normal septate-like junctions (arrowheads), whereas the adjacent loops lack intact septa. Analysis of longitudinal sections of optic nerves from P20 WT mice (F) revealed intact paranodes with normal transverse bands (F, arrowheads). Optic nerves of age-matched KO (G), in contrast, contained numerous disorganized paranodes with everted paranodal loops and irregular transverse bands (G, arrowheads). Bars: A, 1 μm; B, 0.5 μm; C, 0.2 μm; D, 0.2 μm; E, 0.25 μm; F and G, 0.1 μm.

of optic nerves from 2-mo-old *mal* KO mice revealed that although the majority of myelin sheaths were normal with respect to myelin sheath thickness, fiber diameter, and g-ratio (unpublished data), KO animals differed from control animals in the amount of cytoplasm within the myelin sheath (Fig. 3 B). In KO animals, oligodendrocyte cytoplasm was not restricted to the inner and external tongue processes as in WT mice, but conspicuous cytoplasmic inclusions were also present within compact myelin (Fig. 3, compare A with B). In some cases, these cytoplasmic inclusions appeared to correspond to terminal oligodendrocyte processes as their presence correlated with a change in the spiraling direction of myelin. Thus, some axons in KO mice appeared to be concentrically surrounded by more than one myelin sheath (Fig. 3, C and D). For quantification, we analyzed ultrathin sections of optic nerves from 2-mo-old KO and WT mice in double-blind experiments (four KO and three WT mice). Approximately 300 randomly selected myelin sheaths from each animal were monitored for the presence of cytoplasmic inclusions in compact myelin. Cytoplasmic domains were found in 11% (± 1.9%) of all analyzed sheaths of KO animals, but were virtually absent (0.5 ± 0.3%) from control animals. Furthermore, most myelin sheaths in optic nerves of KO mice lacked a well-developed periaxonal oligodendrocyte cytoplasmic collar (Fig. 3, B–D), whereas the majority of myelin sheaths in WT mice had a periaxonal cytoplasmic collar that spanned more than half of the axonal circumference (Fig. 3 A). Our results show that MAL deficiency leads to the formation of morphologically aberrant myelin sheaths, suggesting impaired axon–glia as well as glia–glia interactions.

Myelination in the *mal*-deficient CNS

Cytoplasmic inclusions similar to those seen in the *mal* KO mice have also been observed in adult *mag*-deficient mice (Bartsch et al., 1995). Because *mag* KOs show a delayed onset of myelination (Bartsch et al., 1997), we investigated whether the cytoplasmic inclusions in *mal*-deficient animals are already evident during development and if there is also a delayed onset of myelination. EM analysis of optic nerves from postnatal day 11 and 20 revealed normal onset of myelinogenesis in *mal* KO mice (Fig. 3 F). Some cytoplasmic inclusions in compact myelin were already evident at P11 (unpublished data). At P20 a considerable number of cytoplasmic inclusions were detected (Fig. 3 F, arrows), indicating that they form during the period of active myelination.

MAL deficiency results in paranodal abnormalities

Detailed analysis of longitudinal sections of optic nerves from KO mice revealed a large number of abnormal para-

nodes, with everted paranodal loops projecting away instead of contacting the axon (Fig. 4). Examination of 94 paranodes from two KO animals (3-mo-old) revealed detached and inversely oriented paranodal loops in the majority of the cases (83 of 94; Fig. 4, B, D, and E), whereas in WT animals (Fig. 4, A and C) everted loops were only observed in 2 of 132 analyzed paranodes (unpublished data). Transverse bands, the hallmark of the paranodal axoglia junction of WT nerves (Fig. 4 C, arrowheads), were less regularly organized in KO mice and consisted of diffuse electron-dense material instead of septa (Fig. 4, D and E; arrowheads). Moreover, septa-like structures were frequently absent under some paranodal loops in KO mice (Fig. 4 D, arrow). In very few KO paranodes, transverse bands were still present and had a normal morphology (unpublished data). These analyses demonstrate that although transverse bands were not completely absent in KO animals, they were disrupted and not discretely organized. In contrast to adult KO, which exhibited paranodal abnormalities in 88% of the sites examined, analysis of optic nerves from 20-d-old KO showed everted paranodal loops in only ~50% of the cases (Fig. 4 G), suggesting that the paranodal junctions were formed normally during development and then disassembled.

MAL deficiency results in molecular disorganization of nodes of Ranvier

Because axoglial contact controls local differentiation of myelinated axons, we performed confocal analyses to determine the localization of nodal (e.g., sodium channel [NaCh]), paranodal (e.g., Caspr and neurofascin 155 [NF155]), and juxtaparanodal (e.g., Kv1.2) proteins. Immunofluorescence analysis of optic nerve sections from adult KO showed a strong reduction in the number of Caspr-positive paranodes as well as in the intensity of the Caspr labeling (Fig. 5 B, overview) when compared with WT animals (Fig. 5 A, overview). Moreover, analysis of the few remaining Caspr-positive paranodes at higher magnification revealed a diffuse distribution of Caspr (Fig. 5 B inset, open arrow). Immunofluorescence analysis of Kv1.2 in the juxtaparanodal membrane also revealed a reduction in staining intensity and in the number of positive juxtaparanodes, as well as some lateral diffusion in KO mice (Fig. 5 D). The number of nodes, indicated by tight clusters of NaCh, was not altered in the mutant (Fig. 5 B). Quantification of the number of Caspr clusters in the paranode and of Kv1.2 clusters in the juxtaparanode revealed a reduction of 70–90% and ~70%, respectively, in KO mice (Fig. 6 A). The number of NaCh clusters was similar in WT and KO mice. Immunofluorescence analysis of NF155, which colocalized with Caspr in WT animals (Fig. 5 E, arrowheads), revealed a similarly strong reduction in staining intensity as observed for Caspr, and was barely detectable in KO mice (Fig. 5 F, overview and inset).

Caspr (arrow) and Kv1.2 (open arrow) strictly delineated paranodal and juxtaparanodal compartments in WT mice (Fig. 5 C). However, in adult KO mice, residual Caspr was often dispersed toward the juxtaparanode and even beyond Kv1.2 localization (Fig. 5 D inset, arrowhead). Analysis of the nodal and paranodal length of the few residual Caspr and Kv1.2 clusters in optic nerve, striatum, and spinal cord revealed that the distance between Caspr clusters was

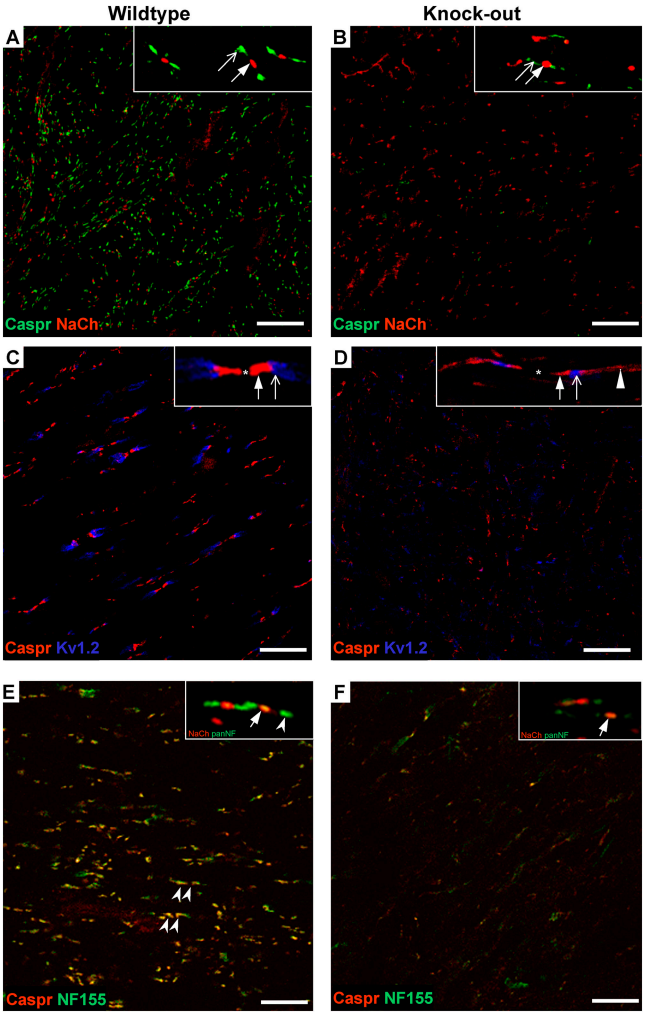

Figure 5. **MAL deficiency leads to reduced expression and dispersed localization of Caspr, Kv1.2, and NF155 at the node of Ranvier.** Confocal localization on longitudinally sectioned optic nerves from 3-mo-old WT (left column) and KO (right column) mice for Caspr (A and B, green; C–F, red), NaCh (A, B, and insets in E and F; red), Kv1.2 (C and D, blue), and NF155 (E and F, green). Note the strong reduction of Caspr and Kv1.2 clusters in KO mice (B and D), whereas the distribution of NaCh was not altered. Inset in D: dispersed distribution of Caspr in *mal*-deficient paranodes, eventually extending beyond juxtaparanodally located Kv1.2 (arrowhead; asterisk; node). However, Kv1.2 (inset in D, open arrow) was never detected within paranodes. NF155 (E and F, green) and Caspr (E and F, red) showed strong overlap (arrowheads point to pairs of clusters) in the paranodes of WT, but were barely detectable in KO mice (inset). Bars, 20 μm.

slightly increased in KO mice when compared with WT animals (Fig. 6 B). In WT mice, the length of nodal NaCh clusters was between 0.61 and 1.39 μm (median 0.85). In comparison, the size of NaCh clusters was slightly increased in KO mice (between 0.97 and 2.21 μm; median 1.59). In line with these data, the distance between two Caspr clusters in WT mice was between 0.96 and 3.52 μm (median 1.79), whereas in *mal* KO mice the distance was between 1.25 and 4.16 μm (median 2.10). Consistent with the observations mentioned above (Fig. 5 D, inset), the length of single Caspr clusters was significantly increased in KO animals ($P < 0.001$); between 0.96 and 3.33 μm with a median of

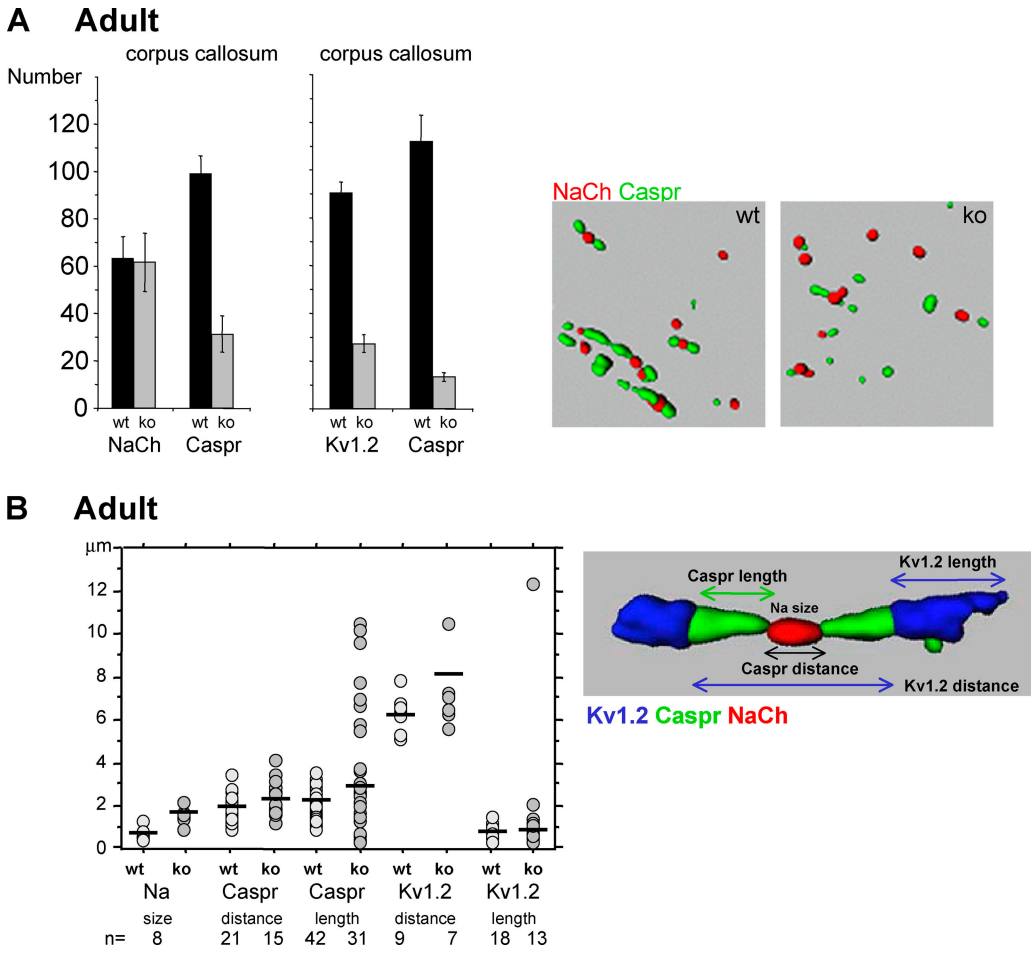

Figure 6. **Quantification of reduced protein clusters in the para- and juxtaparanodal compartments in adult and during development.** (A) Confocal three-dimensional reconstruction analyses of sagittal sections from brains of a 3-mo-old WT and KO mouse for NaCh, Caspr, and Kv1.2. The mean number of particles larger than 1 μm^3 in a total tissue volume of 73 × 73 × 7.5 µm from the longitudinally cut corpus callosum was quantified and graphically shown for NaCh and Caspr costaining (mouse monoclonal anti-pan NaCh [red], rabbit polyclonal anti-Caspr [green]). Note the strong reduction of Caspr cluster pairs, whereas the amount of NaCh was not altered in KO mice. Quantitative immunofluorescent intensity analysis for Caspr and Kv1.2 (rabbit polyclonal anti-Caspr, mouse monoclonal anti-Kv1.2) showed comparable reduction in KO mice. (B) Semiquantitative analysis of nodal, paranodal, and juxtaparanodal length of residual Caspr and Kv1.2 clusters in spinal cord visualized by a bivariate scattergram. The size of NaCh clusters, the distance between a pair of Caspr clusters, the distance between two Kv1.2 clusters, and the length of Kv1.2 clusters was measured. Median: horizontal bar; *n* = number of analyzed clusters.

2.06 in WT mice and between 0.43 and 10.46 µm with a median of 2.64 in KO mice. Interestingly, there is one group of data points that corresponds well to the WT situation, and a second group of values that were much higher that may reflect the dispersed localization of Caspr into the juxtaparanodal region. In line with this observation, the distance between the Kv1.2 clusters was also increased; in WT mice the distance was between 5.17 and 7.89 µm with a median of 6.42 and in KO mice between 5.68 and 10.5 µm with a median of 7.11, supporting our observation that Kv1.2 is not translocated into the paranodal region. The length of Kv1.2 clusters was for most of the measurable clusters comparable to those seen in WT animals with few exceptions, as illustrated in Fig. 6 B. Notably, nodal and paranodal size were quite constant in WT mice, but highly variable in KO. This result is probably related to the fact that Caspr and Kv1.2 were strongly reduced in KO mice and, therefore, only small numbers of clusters could be analyzed. Our results demonstrate that MAL is required for a normal molecular organization of the paranodal and juxtaparanodal region of myelinated axons.

Normal formation but impaired maintenance of paranodes in *mal* KO mice

To examine further whether the paranodal abnormalities observed in *mal*-deficient mice result from the inability of these fibers to establish normal axoglial contacts during development or are the result of later disassembly of the paranodal junction, we compared the distribution of paranodal components between WT and KO mice at different postnatal ages. Immunohistochemical analysis of mice at P16 revealed that in the cerebellum, myelinated fibers expressed proteolipid protein (PLP) as well as MAL (Fig. 7, B and F). In contrast, in the corpus callosum, myelinated fibers expressed PLP (Fig. 7 A, arrows), but do not yet MAL (Fig. 7 E). Immunofluorescence analysis of Caspr showed paranodal clustering in the corpus callosum of P16 WT as well as in KO animals (Fig. 7, I and K; top), suggesting that during

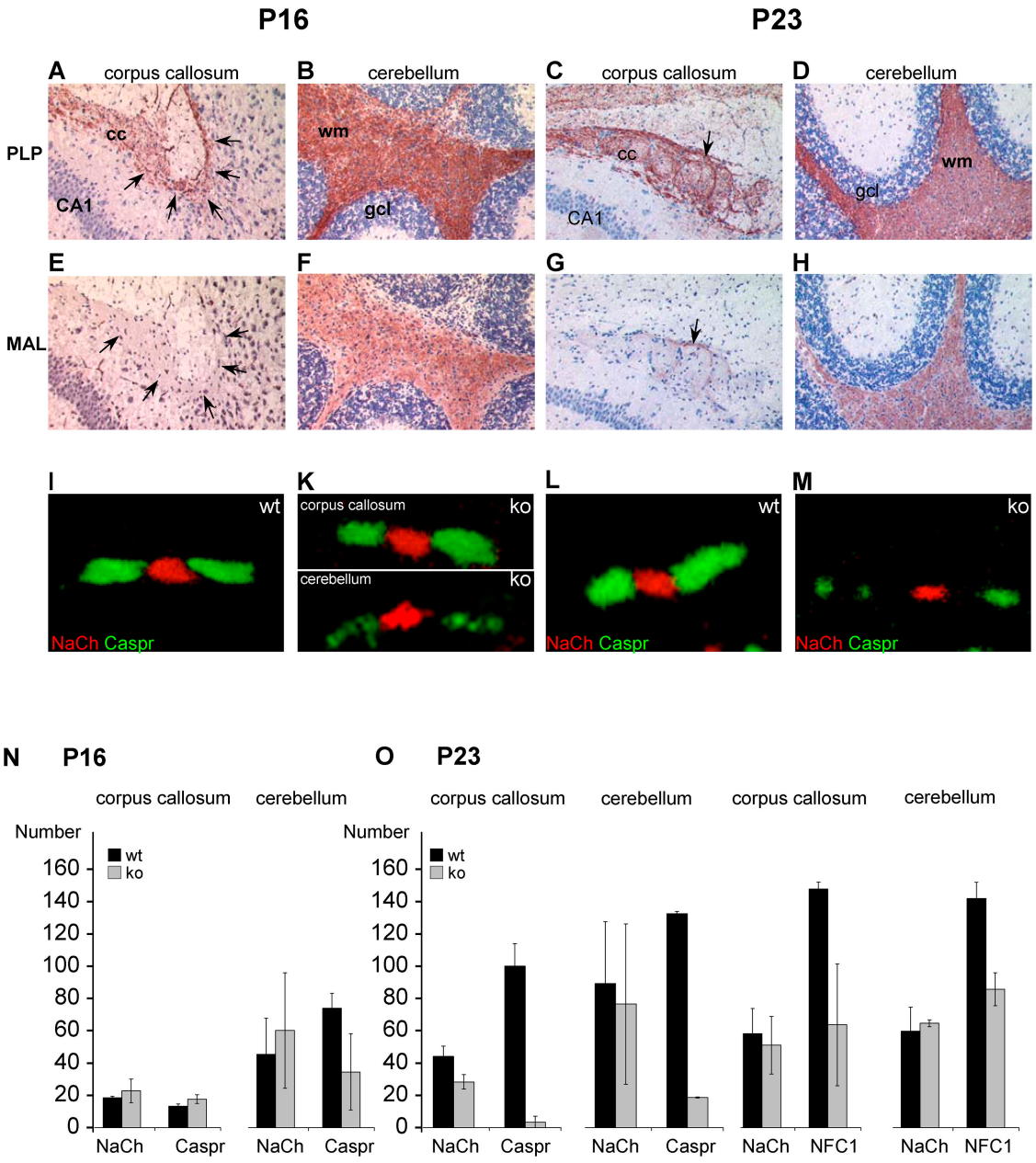

Figure 7. **Onset of paranodal alterations correlates with MAL expression.** Immunohistochemical analysis of sagittal brain sections for PLP (A–D), MAL (E–H), and confocal localization analyses of NaCh (I–M, red) and Caspr (I–M, green) on consecutive tissue sections in WT (A–I and L) and KO mice (K and M). At P16 in WT mice, myelination had already started in the corpus callosum as seen by PLP expression (A, arrows demarcate the border between corpus callosum and hippocampus), but MAL is not detectable yet (E). Clustering of Caspr in paranodes is normal in KO mice (K, top), whereas in the cerebellum myelination is more advanced, as seen by MAL expression (F); the immunofluorescent signal for Caspr is reduced (K, bottom). In contrast, at P23 MAL expression starts in corpus callosum (G, arrow) and Caspr is strongly reduced in paranodes of KO mice (M). PLP expression in KO mice occurred normally (not depicted), comparable to WT mice (C, arrow). Quantification of the confocal localization analyses of NaCh, Caspr, and NF in corpus callosum and cerebellum at P16 (N) and P23 (O). Immunofluorescent particles larger than 0.7 μm^3 were quantified in two WT and KO mice. Note that at P16, total amounts of Caspr were reduced in cerebellum of KO mice, but not in corpus callosum; no differences were observed for NaCh. Error bars: SD from two animals per age and tissue area. At P23, strong reduction of Caspr and NF was observed in cerebellum as well in corpus callosum. For quantification, the pan-NF antiserum was used, which recognizes the 186 (nodal) and 155 (paranodal) isoforms; therefore, the residual amounts of NF-immunofluorescent intensity can be attributed to the nodal 186 isoform, which did not show differences between WT and KO mice (not depicted). wm, white matter; gcl, granule cell layer; CA1, pyramidal cell layer (hippocampus); cc, corpus callosum.

development Caspr clustering occurred normally in the KO. In contrast, at this age, myelination and node formation in the cerebellum was more advanced, as indicated by the higher number of NaCh and Caspr clusters (Fig. 7 N). However, in the cerebellum of P16 KO mice, Caspr was already dispersed and the immunofluorescence signal was weaker (Fig. 7 K, bottom) than in age-matched WT mice (Fig. 7 I). Quantification of Caspr clusters showed a reduction in the cerebellum of P16 KO mice, whereas in the corpus callosum no difference between WT and KO could be

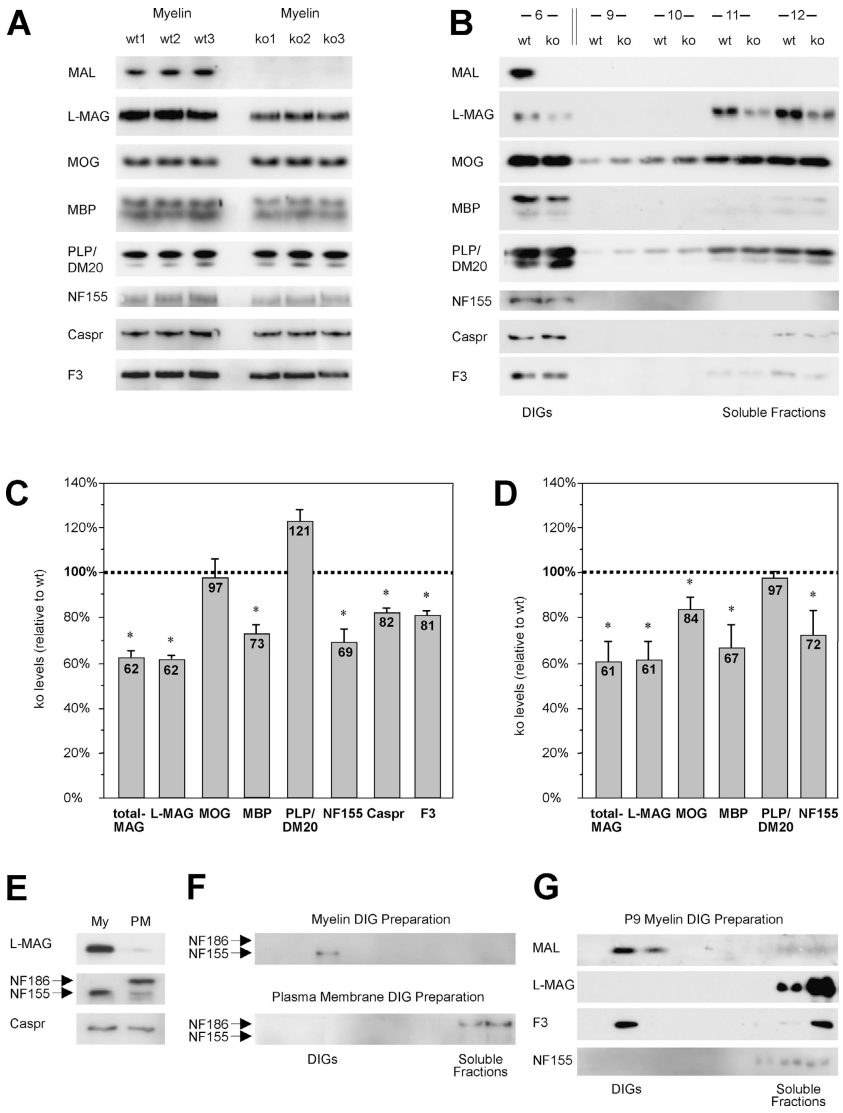

Figure 8. **Alterations in myelin and raft component incorporation in *mal* KO mice.** (A) Western blot analysis of myelin proteins from 4-mo-old WT and KO mice. Brain myelin from three animals of each genotype. Note besides the absence of MAL in KO mice, reduced protein levels of L-MAG, MBP, NF155, and Caspr in the mutants. (B) Western blot analysis of myelin DIG preparations. CHAPS extraction and sucrose step gradient ultracentrifugation from myelin preparations (12 collected gradient fractions). Fraction 1–5: low density (5% sucrose, not depicted); fraction 6: 5%/30% sucrose transition zone with the floating DIGs, fractions 7–10 contain ~30% sucrose (7–8 not depicted), and fraction 11 and 12 contain the detergent-soluble proteins in 40% sucrose. Quantification of myelin proteins in myelin (C) and myelin DIG (D) preparations from KO mice. The relative protein levels in brain myelin (A) and in CHAPS-insoluble fraction 6 (B) were quantified. Values express the percentage of protein in KO compared with WT samples (*, $P < 0.05$). (E) Western blots of L-MAG, Caspr, and both NF isoforms 155 and 186 in myelin and plasma membrane preparations of 4-mo-old WT mouse brain. (F) CHAPS extraction and sucrose step gradient ultracentrifugation from myelin and plasma membranes of WT mice. (G) CHAPS extraction and sucrose step gradient ultracentrifugation from brain myelin preparation of P9 WT mice. In contrast to contactin/F3, L-MAG and NF155 are localized in the soluble fractions. Note that at this developmental stage the extent of myelination differs significantly between brain regions; small amounts of MAL were detectable in the lower brainstem.

detected (Fig. 7 N). At P23, beside PLP, MAL was also expressed in the corpus callosum (Fig. 7, C and G, respectively) and cerebellum (Fig. 7, D and H), and a reduced number of Caspr as well as NF155 clusters was observed in both brain regions (Fig. 7 O). At this age, a dispersed Caspr immunofluorescence was also apparent in paranodes of the corpus callosum of KO mice (Fig. 7 M).

Incorporation of MAG, MBP, and NF155 into CNS myelin depends on MAL

To search for an explanation of the phenotype observed in myelinated CNS axons of *mal*-deficient mice, and based on the hypothesis that the function of MAL as a component of rafts in regulating protein sorting and trafficking might be affected, we quantified the levels of myelin proteins in myelin and in myelin raft preparations of KO and WT animals (Fig. 8). Myelin from brains of 4-mo-old mice ($n = 3$) was analyzed by Western blot analysis (Fig. 8 A). We compared the relative protein levels in WT and KO animals for the compact myelin proteins PLP/DM20 and myelin basic protein (MBP), the two noncompact myelin proteins myelin-associated glycoprotein (MAG) and myelin oligodendrocyte glycoprotein (MOG), and the transmembrane protein NF155 and its binding partner contactin/F3 and Caspr (Fig. 8 C). MAG levels, the 72-kD isoform of MAG (L-MAG), and MBP were significantly reduced to ~60% in myelin derived from KO mice compared with WT samples (Fig. 8 C). As in our confocal analyses, NF155 protein levels were reduced in myelin membranes from KO animals (Fig. 8 A), and Caspr and contactin/F3 were also consistently reduced to ~80% (Fig. 8, A and C). In contrast, the amount of PLP/DM20 in myelin membranes of KO animals was slightly increased, whereas MOG incorporation into KO myelin was not affected (Fig. 8 C).

Next, we examined the effects of *mal* deficiency on myelin rafts and their protein content (Fig. 8 B). CHAPS-resistant DIGs were isolated from all myelin samples mentioned above by detergent extraction and sucrose gradient centrifugation (Fig. 8 B). Rafts accumulated almost exclusively in fraction 6. This observation was independent of the genotype of the animals, indicating that MAL is not crucially required for raft formation. Fraction 6 was used for quantification to compare the raft association of selected proteins in KO and WT mice (Fig. 8 D). *Mal*-deficient DIGs showed decreased

levels of L-MAG protein, but a reduction was also seen in the detergent-soluble fractions (Fig. 8 B, F11 and F12). This indicates that the biochemical association of L-MAG with rafts in myelin membrane preparations, despite overall reduced L-MAG levels, is not directly affected by the lack of MAL. Interestingly, MBP, NF155, and MOG levels were also significantly reduced in myelin-derived DIGs from KO brains, whereas levels of PLP/DM20 remained unchanged (Fig. 8 D). As suggested in Fig. 8 B, more MOG was detected in the detergent-soluble fractions (F11 and F12) in KO mice, indicating that the biochemical properties of *mal*-deficient myelin rafts might be altered for MOG incorporation.

Western blot analysis of DIGs isolated from myelin membranes revealed that NF155 was exclusively recruited into the insoluble fractions and its incorporation was reduced in KO animals (Fig. 8, B and D). Interestingly, contactin/F3, a DIG component of myelin membranes (Kramer et al., 1997), as well as Caspr, showed reduced levels in these insoluble fractions. Because Caspr is only expressed in axons, we tested our myelin membrane preparations for "axonal" plasma membrane contamination. Western blot analysis of myelin membranes compared with plasma membrane fractions showed that pure axonal membrane proteins such as NF186 (localized at the node of Ranvier) were only detected in the plasma membrane preparation (Fig. 8 E). In contrast, NF155 was found almost exclusively in the myelin membrane fractions, comparable to MAG (Fig. 8 E). Interestingly, Caspr was detected in both membrane preparations, suggesting that the DIG-associated part of Caspr may be included in the myelin membrane fraction. Comparable results were obtained for contactin/F3 (unpublished data; Menon et al., 2003). Further characterization of the different neurofascin isoforms showed that NF186 was only present in the soluble fractions in DIG preparations of plasma membrane preparations, whereas NF155 was exclusively found in the insoluble fractions of myelin membranes (Fig. 8 F). Thus, we conclude that NF155, a protein implicated in the formation of the paranodal septate junction (for review see Poliak and Peles, 2003; Salzer, 2003), is associated with lipid rafts, and that its incorporation into myelin membrane may be dependent on MAL. Our data are consistent with and support the idea that NF155 is important for axon–glia interactions and stabilization (Schafer et al., 2004).

NF155 is recruited to rafts during myelin maintenance

From our work, we conclude that paranodes are formed normally during development in *mal*-deficient mice, but become destabilized during myelin maintenance. Our results also demonstrate that NF155 is strongly reduced at the paranodes and to a lesser extent in myelin membranes of KO animals. Thus, MAL may be important for sorting of NF155 to the paranodes in the adult. This is supported by the fact that in the adult, NF155 is solely found in rafts from myelin membranes. Because NF155 is expressed during myelination and paranode formation, we examined whether NF155 is found in rafts during these early stages of axon–glia interactions. We examined DIG preparations from P9 myelin membranes isolated from whole WT mouse brains (Fig. 8 G). In agreement with previous reports, MAL was only present in the insoluble fractions, whereas contactin/F3 was mainly found in the insoluble fractions (Kramer et al., 1999). NF155 as well as L-MAG were only detected in the soluble fractions, indicating that during the early phases of myelin formation NF155 and L-MAG are not recruited to rafts. Our results are consistent with the idea that raft-mediated sorting by MAL plays an important role in the trafficking of particular myelin proteins, such as NF155 and MAG, to the paranodes, and for the stabilization of paranodes in the adult.

Discussion

During myelinogenesis, oligodendrocytes produce myelin at a rate that ranks amongst the highest of all known cellular membrane-producing systems. In the adult, the maintenance of the myelin sheath with its different compartments requires a multifarious system of myelin protein and lipid turnover. MAL (VIP17/MVP17) is suggested to play an important role in sorting and trafficking of particular protein–lipid microdomains, so-called rafts, in myelinating cells. This idea is based on the fact that MAL is associated with the lipid raft forming glycosphingolipids (Frank et al., 1998; Erne et al., 2002), and is required for apical protein sorting in polarized epithelial cells (Cheong et al., 1999). We have investigated the functional role of the raft-associated protein MAL by targeted gene disruption. Our analysis of *mal*-deficient mice demonstrates that maintenance of axon–glia interactions in the CNS is dependent on MAL. Major alterations on the structural level include aberrant inclusions of cytoplasm within compact CNS myelin. Furthermore, paranodal loops at the node of Ranvier are detached from the axon and face away from it. Strong reduction and diffuse distribution of the paranodal protein Caspr and of the potassium channel Kv1.2 at the juxtaparanode was also detected. On the molecular level, we found reduced amounts of MAG, MBP, and NF155 in myelin and raft preparations. During development, paranode formation occurred normally and the onset of paranodal malformation correlated with the normal start of MAL expression in WT mice. These findings demonstrate that MAL plays an important role in the maintenance of normal axon–glia interactions at CNS paranodes.

A particularly striking observation in our work was the effect of MAL deficiency on the paranodal and juxtaparanodal localization of Caspr and Kv1.2, respectively. Because MAL is expressed in the brain exclusively by oligodendrocytes, we hypothesize that lack of MAL is causing altered axon–glia interactions that in turn lead to the drastic changes of Caspr clustering in the paranodal and of Kv1.2 in juxtaparanodal axonal membranes. NF155 is an excellent candidate to cause these impaired axon–glia interactions. This cell adhesion molecule is located at the glial side of the paranodal junction (Tait et al., 2000), is associated with the Caspr–contactin complex (Charles et al., 2002; Gollan et al., 2003), and is markedly reduced in the absence of paranodal septa (Bhat et al., 2001; Boyle et al., 2001; Poliak et al., 2001). Our proposal is based on the finding that NF155 is almost absent in paranodal loops and is recruited to rafts, identifying it as a potential candidate for MAL-mediated sorting. However, we cannot rule out the possibility that the reduction of NF155 in paranodal loops is a consequence of altered MAL-mediated trafficking of a yet unknown component. Nevertheless, our hypothesis

that rafts containing NF155 may play an important role in stabilization and maintenance of the paranodal integrity is in line with the recently proposed model for lipid raft–dependent paranode formation (Schafer et al., 2004).

Many of the molecular alterations at the node of Ranvier of *mal* KO mice are reminiscent of those observed in *cgt*, *cst*, *mag/cgt*, and *cd9* KO mice (Coetzee et al., 1996; Bartsch et al., 1997; Dupree et al., 1998; Honke et al., 2002; Marcus et al., 2002; Ishibashi et al., 2004). However, a major difference is that the outward-facing paranodal loops do not lead to translocation of Kv1.2 from the juxtaparanodes to the paranodes. Also in contrast to those mutant mice, which completely lack paranodal septa, there are some structures reminiscent of septa in *mal*-deficient mice. The latter difference is consistent with the fact that most paranodal loops in *mal*-deficient mice remained closely attached to the axon, whereas the other mutant mouse lines displayed larger gaps between oligodendrocytes and axons. Another important difference is that we observed alterations only in the CNS, whereas the adult PNS did not seem to be affected by the lack of MAL. This could be due to compensatory mechanisms of another as yet unknown raft-associated proteolipid protein, which might replace the functional role of MAL, or known basic structural differences between myelinated PNS and CNS nerve fibers (Salzer, 2003).

Because MAL is associated with sulfatides (Frank et al., 1998), and lack of sulfatides leads to similar paranodal malformation as seen in our mutants (Honke et al., 2002), we investigated the lipid composition of myelin and plasma membranes in *mal*-deficient mice. No major alterations in the amounts of sulfatides, galactosylceramide (GalC), or cholesterol were found (unpublished data). Still, it is intriguing that *mal*-deficient mice display some pathological alterations that are also seen in mice lacking ceramide galactosyl transferase (CGT), CST, MAG, CGT and MAG, or CD9 (Poliak and Peles, 2003). Thus, these molecules may play overlapping roles in mediating axon–glia interactions, either by having a function in the sorting and trafficking of the receptor molecules involved or by having receptor properties themselves. Another important common feature shared by these mutants is that the paranodes form normally and independently of MAL (this paper), MAG (Marcus et al., 2002), or galactolipids (Dupree et al., 1998; Ishibashi et al., 2002), but destabilize over time in their absence. Therefore, MAL, MAG, and the galactolipids are not necessary for the initial interactions between the oligodendrocyte and the axon, but rather contribute to the stabilization of CNS paranodes. Consistent with this idea, we show that during the early phases of myelination, clustering of Caspr and NF155 in the paranodes occurred normally in *mal*-deficient mice. However, at the time when MAL would have been expressed in myelin membranes, the number of Caspr and NF155 clusters was strongly reduced, and on the ultrastructural level, we observed an increasing number of everted paranodal loops. Thus, distinct molecular mechanisms appear to be responsible for the formation and the maintenance of axon–glia interactions at the paranode. Beside NF155, MAG may also play a major role in this maintenance process, possibly by stabilizing myelin membrane interactions directly in the paranodal region, as MAG is expressed at low levels in CNS paranodal loops (Bartsch et al., 1989). Alternatively, MAG may mediate internodal axon–glia interactions because it is expressed in the periaxonal myelin membrane (Schachner and Bartsch, 2000). MAL is predominantly located in compact myelin (Schaeren-Wiemers et al., 1995b; Frank et al., 1998), but it was also found in noncompacted compartments such as Schmidt-Lanterman incisures in the PNS where it colocalizes with MAG (Erne et al., 2002). Whether MAL and MAG are colocalized in paranodal membranes in the CNS could not be elucidated yet due to the lack of suitable reagents. Analysis of MAG in myelin membranes as well as CHAPS-insoluble DIGs isolated from KO and WT brain myelin showed a comparable reduction of 40% in the mutant, indicating that within the myelin membrane of the mutant brain, MAG appears to be still surrounded by (or interacting with) a comparable subset of myelin lipids. Thus, MAL may play a functional role in sorting and trafficking of MAG that is not dependent on its raft association in myelin membranes. However, the sorting and trafficking mechanisms for myelin membrane proteins are not yet fully understood. The reduction of the total amounts of MAG could either be due to a less efficient transport to the myelin membranes or to reduced protein synthesis. Analysis of whole-brain homogenates revealed a comparable reduction of MAG as in myelin membranes (unpublished data) excluding accumulation of MAG in the oligodendrocyte endosomal/lysosomal system. Furthermore, quantitative RT-PCR analysis of four 3-mo-old WT and four age-matched KO animals did not show a reduction in S- or L-MAG mRNA expression levels in the brain of *mal*-deficient mice (unpublished data). Therefore, the remaining protein may undergo rapid or enhanced degradation in the absence of MAL.

GalC and sulfatide account for one third of the myelin lipids and are enriched in lipid rafts. Hence, lack of MAL may impair efficient trafficking of glycolipids such as GalC and sulfatides particularly to the paranodal compartment at the time when the axon–glia contacts should be stabilized. According to the model of Schafer et al. (2004), galactolipids may have an important role in stabilization of axon–glial contacts by promoting the formation of NF155-containing lipid rafts during myelin maintenance. This conclusion is based on the observation that the absence of GalC or sulfatides results in paranodal disruption and concurrent reduction of NF155-containing lipid rafts (Schafer et al., 2004). From our work, we cannot elucidate whether the GalC and sulfatide levels in the paranode *mal* KO mice differ from that of WT animals. Less GalC and/or sulfatides might be incorporated into the "paranodal lipid rafts," and therefore impair stabilization. Interestingly, a recent report suggests that GalC levels may directly regulate MAL expression. In the arylsulfatase KO animals, beside an accumulation of sulfatide, there are reduced levels of GalC in myelin membranes accompanied by reduced expression levels of MAL protein and mRNA (Saravanan et al., 2004). In contrast, overexpression of CGT led to an increase in MAL expression and to an enrichment of MAL in myelin membranes (unpublished data). The expression of other myelin proteins such as PLP, MBP, and MAG was not affected, indicating that a tight balance between galactolipids (particularly GalC) and MAL levels exists that may be important for the

formation of particular lipid rafts or plasma membrane microdomains.

In conclusion, we demonstrate that the raft-associated myelin protein MAL plays an important role in the maintenance of the myelin sheath and in normal axon–glia and glia–glia membrane interactions, suggesting that lipid rafts within particular oligodendrocyte compartments may be critical for the maintenance of the axon–myelin sheath integrity.

Materials and methods

Generation of *mal*-deficient mice

The gene-targeting vector was generated by insertion of a *lac*Z/neomycin cassette within exon 1 of *mal* (Fig. 1 A). Appropriate genomic fragments were isolated from cosmid 2.1 (Magyar et al., 1997). The *lac*Z/Neo cassette was derived from plasmid p1049 (a gift from Dr. Bill Wisden, Medical Research Council Centre, Cambridge, UK) and was inserted in frame after the third codon of the *mal* gene. An HSV-Tk selection cassette (derived from the Tk/Neo/UMS-vector; a gift from Dr. Charles Weissman, University College London, London, UK) was added for negative selection. 129/Ola-derived embryonic stem cells (Magin et al., 1992) were transfected with the NotI-linearized construct by electroporation and were selected with G418 and gancyclovir. Surviving and putatively targeted embryonic stem cell clones were screened using PCR. The oligonucleotides 5′-AGGGCGATTAAGTTGGCTAAC-3′ (hybridizes to *lac*Z) and 5′-GCAGGGCTACCAAGTTGTAAG-3′ (binds to the XbaI–XbaI fragment upstream of the construct; Fig. 1 A) yielded a 1.3-kb product in correctly targeted clones. Gene targeting was confirmed by Southern blotting of EcoRV-digested genomic DNA using XbaI–XbaI (5′ probe; Fig. 1 A) as a probe. Single integration was established by subsequent hybridization with a *lac*Z probe.

Tissue and myelin preparations

Mice were decapitated and tissues were rapidly dissected and either used directly or snap-frozen at −80°C for myelin preparation, or embedded in O.C.T. compound (Miles Laboratory) and frozen on dry ice for immunohistochemistry. For paraffin embedding, tissues were fixed in 4% PFA, dehydrated, and embedded in Paraplast Plus (Sherwood Medical). Tissues for EM were either perfusion fixed (Bartsch et al., 1995) or immersed in a modified Karnovsky solution (Annefeld et al., 1990). For postfixation with osmium tetroxide, dehydration, and Epon embedding, see Bartsch et al. (1995).

Myelin membrane isolation and preparation of CHAPS detergent extracts were performed as described previously (Erne et al., 2002).

Antibodies

Anti-MAL rabbit antiserum was raised against a recombinant GST-coupled polypeptide comprising the 53 NH_2-terminal amino acids of MAL (GST-TM1) and was affinity purified. Additional rabbit pAbs were used as follows: anti-L-MAG (Erb et al., 2003), anti-PLP (from Dr. K.-A. Nave, Max-Planck-Institute of Experimental Medicine, Göttingen, Germany), anti-Caspr (from Dr. E. Peles, Weizmann Institute of Science, Rehovot, Israel), anti-NF155 and anti-NF155/186 (from Dr. P. Brophy, University of Edinburgh, Edinburgh, UK), and anti-contactin/F3 (from Dr. J. Trotter, Johannes Gutenberg University, Mainz, Germany). Monoclonal mouse antibodies were as follows: Anti-MBP (130–137; Boehringer), anti-MAG (C513; Boehringer), anti-MOG (from Dr. R. Reynolds, Imperial College London, London, UK), anti-NaCh (Sigma-Aldrich), anti-Caspr (from Dr. E. Peles), and anti-Kv1.2 (Upstate Biotechnology). Secondary antibodies for immunohistochemical and Western blot analysis were as follows: Goat anti–mouse IgG-peroxidase, goat anti–rabbit IgG-peroxidase (Sigma-Aldrich), ABC Elite anti–mouse and anti–rabbit kit (Vector Laboratories), goat anti–mouse IgG-Cy3, goat-anti-rabbit IgG-Cy2, goat anti–mouse IgG-Cy5 (Jackson Laboratories), and goat anti–rabbit IgG-Alexa 488 (Molecular Probes, Inc.).

Immunohistochemistry, fluorescence confocal microscopy, and EM

Cryostat sections of fresh frozen tissues (7–10 μm) were mounted on gelatin/chromalaun-coated slides, dried at RT, and fixed for 1 h in 10% buffered formalin solution. Permeabilization with 70% ethanol was done overnight at RT (Caspr and Kv1.2 immunohistochemistry). For anti-NaCh stainings, tissue sections were fixed in methanol for 20 min at −20°C. Paraffin sections (5 μm) were dried overnight and processed (Erne et al., 2002). LacZ staining was performed as described previously (Leone et al., 2003).

Double staining for confocal fluorescence microscopy was performed by incubating tissues with primary antibodies overnight at 4°C or for 1 h at RT. Sections analysis: inverted scanning confocal microscope (LSM 510; Carl Zeiss MicroImaging, Inc.). 1-μm optical sections were transferred to a silicon graphics workstation (Silicon Graphics Inc.) for processing with Imaris software (Bitplane AG). Cluster counting for Caspr, NF155/186, Kv1.2, and NaCh was performed by acquiring confocal image stacks with a constant volume of 73 × 73 × 7.5 μm and constant detection sensitivities. Particles were extracted and reconstructed using constant threshold values and voxel resolution in the Imaris surpass program. Particles with sizes lower than 0.7 μm^3 were excluded. The number of clusters within a stack were averaged over 6–10 stacks per animal, section, and area (two animals). Transmission microscopy was performed on a microscope (DMRE, Leica). Ultrastructural analysis of tissues was performed with a transmission electron microscope (Morgani 268D; Philips). Fiber diameter, myelin sheath thickness, and g-ratio of optic nerve fibers were measured in 100 fibers from each genotype with the AnalySIS image analysis system (Soft Imaging System GmbH).

SDS-PAGE and Western blot analysis

Protein samples were separated on 15% polyacrylamide gels (8% for MAG, contactin/F3, caspr, and NF155/186; Erne et al., 2002).

Quantification of Western blot results

To achieve a linear relation between the amount of analyzed myelin protein and the resulting signal intensity, the optimal range of analyzed myelin protein was determined for each antibody used. Within this range, five different amounts (5, 4, 3, 2, and 1 μg) from a WT and a KO myelin protein pool ($n = 3$) were analyzed in parallel on the same blot. Signal intensities were analyzed with the MultiImage cabinet and camera (Alpha Innotech Corporation), and were quantified with the "Spot Denso" module of the Chemilmager v5.5 software. Signal intensities were plotted against the amount of analyzed myelin protein (or DIGs), and trend lines through the values obtained for WT and KO samples were added. The ratio of the slopes of KO and WT trend lines reflects the amount of the analyzed myelin protein in the KO relative to the WT pool (Fig. 8 D). For statistical analysis, single WT and KO signal intensities from the dilution series were extrapolated to 100% of analyzed myelin or DIGs for each experiment. The mean value of all experiments with SDs and P values (*t* test) were determined for each experiment.

We thank B. Kaisling and J. Loffling, T. Magin, R. Martini, P. Brophy, E. Peles, and S. Sansano and J. Caduff for their crucial contributions.

This work was supported by the Swiss National Science Foundation (to N. Schaeren-Wiemers and U. Suter), the Roche Research Foundation (to N. Schaeren-Wiemers), the Swiss Muscle Disease Foundation, the National Center of Competence in Research "Neural Plasticity and Repair", and the Swiss Bundesamt for Science related to the Commission of the European Communities, specific RTD program "Quality of Life and Management of Living Resources," QLK6-CT-2000-00179 (to U. Suter).

Submitted: 15 June 2004
Accepted: 14 July 2004

References

Annefeld, M., B. Erne, and Y. Rasser. 1990. Ultrastructural analysis of rat articular cartilage following treatment with dexamethasone and glycosaminoglycan-peptide complex. *Clin. Exp. Rheumatol.* 8:151–157.

Arroyo, E.J., and S.S. Scherer. 2000. On the molecular architecture of myelinated fibers. *Histochem. Cell Biol.* 113:1–18.

Bartsch, S., D. Montag, M. Schachner, and U. Bartsch. 1997. Increased number of unmyelinated axons in optic nerves of adult mice deficient in the myelin-associated glycoprotein (MAG). *Brain Res.* 762:231–234.

Bartsch, U., F. Kirchhoff, and M. Schachner. 1989. Immunohistological localization of the adhesion molecules L1, N-CAM, and MAG in the developing and adult optic nerve of mice. *J. Comp. Neurol.* 284:451–462.

Bartsch, U., D. Montag, S. Bartsch, and M. Schachner. 1995. Multiply myelinated axons in the optic nerve of mice deficient for the myelin-associated glycoprotein. *Glia.* 14:115–122.

Bhat, M.A., J.C. Rios, Y. Lu, G.P. Garcia-Fresco, W. Ching, M. St Martin, J. Li, S. Einheber, M. Chesler, J. Rosenbluth, et al. 2001. Axon-glia interactions and the domain organization of myelinated axons requires neurexin IV/Caspr/Paranodin. *Neuron.* 30:369–383.

Boyle, M.E., E.O. Berglund, K.K. Murai, L. Weber, E. Peles, and B. Ranscht.

2001. Contactin orchestrates assembly of the septate-like junctions at the paranode in myelinated peripheral nerve. *Neuron.* 30:385–397.

Charles, P., S. Tait, C. Faivre-Sarrailh, G. Barbin, F. Gunn-Moore, N. Denisenko-Nehrbass, A.M. Guennoc, J.A. Girault, P.J. Brophy, and C. Lubetzki. 2002. Neurofascin is a glial receptor for the paranodin/Caspr-contactin axonal complex at the axoglial junction. *Curr. Biol.* 12:217–220.

Cheong, K.H., D. Zacchetti, E.E. Schneeberger, and K. Simons. 1999. VIP17/MAL, a lipid raft-associated protein, is involved in apical transport in MDCK cells. *Proc. Natl. Acad. Sci. USA.* 96:6241–6248.

Coetzee, T., N. Fujita, J. Dupree, R. Shi, A. Blight, K. Suzuki, and B. Popko. 1996. Myelination in the absence of galactocerebroside and sulfatide: normal structure with abnormal function and regional instability. *Cell.* 86:209–219.

Dupree, J.L., T. Coetzee, A. Blight, K. Suzuki, and B. Popko. 1998. Myelin galactolipids are essential for proper node of Ranvier formation in the CNS. *J. Neurosci.* 18:1642–1649.

Erb, M., A.J. Steck, K.A. Nave, and N. Schaeren-Wiemers. 2003. Differential expression of L- and S-MAG upon cAMP stimulated differentiation in oligodendroglial cells. *J. Neurosci. Res.* 71:326–337.

Erne, B., S. Sansano, M. Frank, and N. Schaeren-Wiemers. 2002. Rafts in adult peripheral nerve myelin contain major structural myelin proteins and myelin and lymphocyte protein (MAL) and CD59 as specific markers. *J. Neurochem.* 82:550–562.

Frank, M. 2000. MAL, a proteolipid in glycosphingolipid enriched domains: functional implications in myelin and beyond. *Prog. Neurobiol.* 60:531–544.

Frank, M., M.E. van der Haar, N. Schaeren-Wiemers, and M.E. Schwab. 1998. rMAL is a glycosphingolipid-associated protein of myelin and apical membranes of epithelial cells in kidney and stomach. *J. Neurosci.* 18:4901–4913.

Frank, M., S. Atanasoski, S. Sancho, J.P. Magyar, T. Ruelicke, M.E. Schwab, and U. Suter. 2000. Progressive segregation of unmyelinated axons in peripheral nerves, myelin alterations in the CNS, and cyst formation in the kidneys of myelin and lymphocyte protein-overexpressing mice. *J. Neurochem.* 75: 1927–1939.

Gollan, L., D. Salomon, J.L. Salzer, and E. Peles. 2003. Caspr regulates the processing of contactin and inhibits its binding to neurofascin. *J. Cell Biol.* 163: 1213–1218.

Honke, K., Y. Hirahara, J. Dupree, K. Suzuki, B. Popko, K. Fukushima, J. Fukushima, T. Nagasawa, N. Yoshida, Y. Wada, and N. Taniguchi. 2002. Paranodal junction formation and spermatogenesis require sulfoglycolipids. *Proc. Natl. Acad. Sci. USA.* 99:4227–4232.

Ishibashi, T., J.L. Dupree, K. Ikenaka, Y. Hirahara, K. Honke, E. Peles, B. Popko, K. Suzuki, H. Nishino, and H. Baba. 2002. A myelin galactolipid, sulfatide, is essential for maintenance of ion channels on myelinated axon but not essential for initial cluster formation. *J. Neurosci.* 22:6507–6514.

Ishibashi, T., L. Ding, K. Ikenaka, Y. Inoue, K. Miyado, E. Mekada, and H. Baba. 2004. Tetraspanin protein CD9 is a novel paranodal component regulating paranodal junctional formation. *J. Neurosci.* 24:96–102.

Kim, T., and S.E. Pfeiffer. 1999. Myelin glycosphingolipid/cholesterol-enriched microdomains selectively sequester the non-compact myelin proteins CNP and MOG. *J. Neurocytol.* 28:281–293.

Kim, T., K. Fiedler, D.L. Madison, W.H. Krueger, and S.E. Pfeiffer. 1995. Cloning and characterization of MVP17: a developmentally regulated myelin protein in oligodendrocytes. *J. Neurosci. Res.* 42:413–422.

Koch, T., T. Brugger, A. Bach, G. Gennarini, and J. Trotter. 1997. Expression of the immunoglobulin superfamily cell adhesion molecule F3 by oligodendrocyte-lineage cells. *Glia.* 19:199–212.

Kramer, E.M., T. Koch, A. Niehaus, and J. Trotter. 1997. Oligodendrocytes direct glycosyl phosphatidylinositol-anchored proteins to the myelin sheath in glycosphingolipid-rich complexes. *J. Biol. Chem.* 272:8937–8945.

Kramer, E.M., C. Klein, T. Koch, M. Boytinck, and J. Trotter. 1999. Compartmentation of Fyn kinase with glycosylphosphatidylinositol-anchored molecules in oligodendrocytes facilitates kinase activation during myelination. *J. Biol. Chem.* 274:29042–29049.

Leone, D.P., S. Genoud, S. Atanasoski, R. Grausenburger, P. Berger, D. Metzger, W.B. Macklin, P. Chambon, and U. Suter. 2003. Tamoxifen-inducible glia-specific Cre mice for somatic mutagenesis in oligodendrocytes and Schwann cells. *Mol. Cell. Neurosci.* 22:430–440.

Magin, T.M., J. McWhir, and D.W. Melton. 1992. A new mouse embryonic stem cell line with good germ line contribution and gene targeting frequency. *Nucleic Acids Res.* 20:3795–3796.

Magyar, J.P., C. Ebensperger, N. Schaeren-Wiemers, and U. Suter. 1997. Myelin and lymphocyte protein (MAL/MVP17/VIP17) and plasmolipin are members of an extended gene family. *Gene.* 189:269–275.

Marcus, J., J.L. Dupree, and B. Popko. 2002. Myelin-associated glycoprotein and myelin galactolipids stabilize developing axo–glial interactions. *J. Cell Biol.* 156:567–577.

Martin-Belmonte, F., R. Puertollano, J. Millan, and M.A. Alonso. 2000. The MAL proteolipid is necessary for the overall apical delivery of membrane proteins in the polarized epithelial Madin-Darby canine kidney and fischer rat thyroid cell lines. *Mol. Biol. Cell.* 11:2033–2045.

Menon, K., M.N. Rasband, C.M. Taylor, P. Brophy, R. Bansal, and S.E. Pfeiffer. 2003. The myelin-axolemmal complex: biochemical dissection and the role of galactosphingolipids. *J. Neurochem.* 87:995–1009.

Poliak, S., and E. Peles. 2003. The local differentiation of myelinated axons at the nodes of Ranvier. *Nat. Rev. Neurosci.* 4:968–980.

Poliak, S., L. Gollan, D. Salomon, E.O. Berglund, R. Ohara, B. Ranscht, and E. Peles. 2001. Localization of Caspr2 in myelinated nerves depends on axon-glia interactions and the generation of barriers along the axon. *J. Neurosci.* 21:7568–7575.

Puertollano, R., F. Martin-Belmonte, J. Millan, M.C. de Marco, J.P. Albar, L. Kremer, and M.A. Alonso. 1999. The MAL proteolipid is necessary for normal apical transport and accurate sorting of the influenza virus hemagglutinin in Madin-Darby canine kidney cells. *J. Cell Biol.* 145:141–151.

Salzer, J.L. 2003. Polarized domains of myelinated axons. *Neuron.* 40:297–318.

Saravanan, V.P.M., N. Schaeren-Wiemers, D. Klein, R. Sandhoff, A. Schwarz, A. Yaghootfam, V. Gieselmann, and S. Franken. 2004. Specific downregulation and mistargetting of the proteolipid protein MAL in a glycolipid storage disorder. *Neurobiol. Dis.* 16:396–406.

Schachner, M., and U. Bartsch. 2000. Multiple functions of the myelin-associated glycoprotein MAG (siglec-4a) in formation and maintenance of myelin. *Glia.* 29:154–165.

Schaeren-Wiemers, N., C. Schaefer, D.M. Valenzuela, G.D. Yancopoulos, and M.E. Schwab. 1995a. Identification of new oligodendrocyte- and myelin-specific genes by a differential screening approach. *J. Neurochem.* 65:10–22.

Schaeren-Wiemers, N., D.M. Valenzuela, M. Frank, and M.E. Schwab. 1995b. Characterization of a rat gene, rMAL, encoding a protein with four hydrophobic domains in central and peripheral myelin. *J. Neurosci.* 15:5753–5764.

Schafer, D.P., R. Bansal, K.L. Hedstrom, S.E. Pfeiffer, and M.N. Rasband. 2004. Does paranode formation and maintenance require partitioning of neurofascin 155 into lipid rafts? *J. Neurosci.* 24:3176–3185.

Simons, M., E.M. Kramer, C. Thiele, W. Stoffel, and J. Trotter. 2000. Assembly of myelin by association of proteolipid protein with cholesterol- and galactosylceramide-rich membrane domains. *J. Cell Biol.* 151:143–154.

Tait, S., F. Gunn-Moore, J.M. Collinson, J. Huang, C. Lubetzki, L. Pedraza, D.L. Sherman, D.R. Colman, and P.J. Brophy. 2000. An oligodendrocyte cell adhesion molecule at the site of assembly of the paranodal axo–glial junction. *J. Cell Biol.* 150:657–666.

Zacchetti, D., J. Peranen, M. Murata, K. Fiedler, and K. Simons. 1995. VIP17/MAL, a proteolipid in apical transport vesicles. *FEBS Lett.* 377:465–469.